Available online at www.sciencedirect.com
SCIENCE DIRECT®
International Journal of Mass Spectrometry 225 (2003) 191–212
International Journal of Mass Spectrometry
www.elsevier.com/locate/ijms

Review

Development of classical trajectory methodology for the study of dissociation dynamics of polyatomic ions

Myung Soo Kim*, Jeong Hee Moon

School of Chemistry, National Creative Research Initiative Center for Control of Reaction Dynamics, Seoul National University, Seoul 151-742, South Korea

Received 30 September 2002; accepted 2 January 2003

Abstract

Classical trajectory method developed to study ion dissociation dynamics is reviewed with emphasis placed on the methods tested, adopted, or developed in this laboratory. A systematic method to construct a potential energy surface from ab initio data is explained in some details. Generally adopted methods for trajectory calculation are described. A newly devised method for reliable calculations of product mode-specific energies from the trajectory results is explained. A scaling theorem for classical dynamics found in this laboratory is presented together with its application to correct for the errors arising from inaccurate ab initio data. Finally, the influence of numerically induced chaos on trajectory is described together with the method to check its appearance as a caution to the misuse of the trajectory method in the long time dynamics.

Keywords: Classical trajectory; Ion dissociation dynamics; Scaling; Numerically induced chaos

1. Introduction

Understanding dissociation dynamics of an internally excited polyatomic cation is one of the central subjects in mass spectrometry. This provides a theoretical basis to the mechanistic interpretation of mass spectra and helps to extract structural information from various spectral data. The knowledge is also important to assess the characteristics and capability of ionization and dissociation methods and provides useful guidelines to improve them. Molecular dissociation is also an important subject in the field of chemical reaction dynamics [1–4]. Emphasis in this field is placed mostly on the neutral rather than ion reactions even though the general theoretical framework to handle the dissociation dynamics is hardly affected by the charge state. Ease of experiment and availability of abundant experimental data may be the main reasons for the bias toward the neutral chemistry.

In the standard theory of mass spectra, or quasi-equilibrium theory (QET), electronic energy acquired by an ion at the time of its formation is assumed to be converted rapidly to vibrational energy in the ground electronic state via radiationless processes such as internal conversion. Rapid intramolecular redistribution of the vibrational energy is also assumed. Then,

* Corresponding author. Tel.: +82-2-880-6652; fax: +82-2-889-1568.
E-mail address: myungsoo@plaza.snu.ac.kr (M.S. Kim).

1387-3806/03/$ – see front matter © 2003 Elsevier Science B.V. All rights reserved.
doi:10.1016/S1387-3806(03)00021-6

the dissociation rate constant is evaluated using the microcanonical transition state theory, or the Rice–Ramsperger–Kassel–Marcus (RRKM) theory [5–10]. Checking the validity of the first assumption, which may be called the assumption of electronic ergodicity, is an active research subject in itself [11,12]. Dissociation in a repulsive electronic state or via curve crossing to a repulsive state is the most common exception to this assumption [13–23]. Study of nonadiabatic transition, for example near the conical intersection, which is a topic of intensive research interest [24–28], has relevance for the test of this assumption. Our recent discovery of very long-lived excited electronic states of several molecular cations suggests that the assumption may not be as generally applicable as was thought previously [11,12,29]. In this review, we will not go into details of this topic but accept the validity of the assumption. Or, we will just focus on the dissociation dynamics of molecular ions prepared in the ground electronic state.

The investigation of ion dissociation dynamics can be divided into two sub-fields. One concerns the rate constant and may be called the entrance channel dynamics. The other concerns the energy partitioning in the products, or the exit channel dynamics. Even though state-selective measurement [30–34] of these properties would be extremely useful for a comparison with theoretical results, hardly any such data are available except for the dissociation of simple diatomic ions. Instead, most of the experimental data reported so far were obtained for energy-selected dissociation.

Photoelectron–photoion coincidence (PEPICO) spectrometry has been the most fruitful technique to measure energy-selected dissociation rate constant [13–18,35,36], and the rate constant of a dissociation occurring on a microsecond time scale can be measured with this technique. The photodissociation kinetics scheme developed in this laboratory allows the measurement of rate constants on a nanosecond time scale [37–42]. In this technique, energy selection is achieved by generating a molecular ion by charge exchange and exciting it with a monochromatic laser. The same technique has been used to measure the kinetic energy release (KER) or its distribution (KERD) [43]. It is to be mentioned, however, that the majority of the experimental KERD data reported was measured for metastable ion decomposition [44] using mass-analyzed ion kinetic energy spectrometry (MIKES) [45,46]. Even though energy selection is not done for the parent ion in this technique, reasonable estimation of its internal energy is possible once the rate–energy data are known.

For a theoretical understanding of a chemical reaction, the time-dependent change of the system must be calculated, which usually requires a tremendous amount of computation. Such a difficulty is avoided in the transition state theory by postulating a statistical hypothesis of quasi-equilibrium between transition state species and reactants. In the usual RRKM–QET [5,6,47–49] calculation of a rate constant, the reaction critical energy and vibrational frequencies of reactants and transition species are needed. However, these parameters are not well known in most of the cases. In practice, experimental rate–energy data are fit with RRKM–QET calculation by adjusting above parameters. The reaction critical energy, E_0, is evaluated from the best fit together with the activation entropy, $\Delta S^{\ddagger}$, which is related to the looseness of the transition state [50,51]. When the transition state is completely loose, or is well-approximated by the orbiting transition state, transition state parameters can be replaced by those of the products alleviating the above ambiguity. However, there are not many reactions which are nearly completely loose such that the orbiting transition states become true bottlenecks. In spite of various deficiencies of the statistical approach, it is the only method which can supply the theoretical rate constant of a reaction occurring on a nanosecond or longer time scale. However, rigorous dynamical approaches are needed to study faster reactions for which the statistical hypothesis may not be valid.

Product energy partitioning, especially the KERD which can be easily measured for ion dissociation, can be calculated with the statistical theories also. In particular, excellent agreement between the experimental and theoretical KERDs is achieved when the reverse critical energy of dissociation is negligible [39,52–54]. RRKM–QET formulated from the perspective of

reverse reaction, which is commonly called the phase space theory [3,52,53,55–57], is widely accepted in such a case. Agreement is not as good when the reverse barrier is not negligible and energy exchange occurs among various degrees of freedom during the exit channel motion. Even though attempts have been made to improve the theoretical prediction by adding various assumptions concerning exit channel coupling [58,59], no statistical approach with a general applicability has emerged yet. Namely, one must resort to rigorous dynamics calculations to account for the experimental energy partitioning data and to understand the exit channel dynamics of a dissociation reaction.

It is appropriate to solve the Schrödinger equation to investigate the dynamics of a molecular system. Significant progress has been made during the past decade to handle this formidable task such as calculations of wave packet propagation by solving time-dependent Schrödinger equation [60–62] or of scattering *S*-matrix by solving the time-independent Schrödinger equation [63–67]. Regardless, the computational demand is still tremendous and an application of the quantum dynamics is limited to five-atom systems at the moment [68,69]. Hence, classical dynamics has been widely used to obtain detailed information on the dissociation processes even though the method is inherently inadequate to account for the quantum phenomena such as tunneling and zero-point effects.

In classical dynamics [1,70], a trajectory, or time evolution of a system in the phase space, is calculated by solving classical equations of motion which are usually in the form of Hamilton's equations. Results from trajectory calculations starting from hundreds, if not thousands of initial phase space points are averaged for a reliable representation of a real situation. Solving the classical equations of motion requires knowledge of the force acting on the atoms in the system along a trajectory. In the conventional approach [71–76], the potential energy surface (PES) covering the reactant, transition state, and product regions, which is called the global PES, is constructed prior to trajectory calculations. Then, as many trajectories as needed or practically feasible are calculated using this surface. An alternative is to obtain the force, or the gradient of the potential energy, on points along a trajectory by ab initio calculation. For example, the dynamic reaction path routine incorporated in ab initio packages [77,78] provides such a capability. The fact that the costly gradient calculation must be done at many points on each trajectory is the major disadvantage of this approach especially when calculation of many trajectories are desired. Some attempts have been made to reduce the computational demand by introducing trust region [79] or local fifth order fitting [80]. The computational demand of the method is still tremendous, however, compared to the conventional one. Recent Gaussian 98 package has incorporated one of the direct dynamics method mentioned above. A review of the trust region dynamics and its application to ion dissociation reactions have been presented recently by Uggerud [81]. A related approach is the Car–Parrinello method which computes energies and densities of valence electrons 'on the fly' by electronic density functional theory [82]. This method has become popular in molecular dynamics and can handle high dimensionality [83–85].

In the present review, the classical trajectory method based on the conventional approach and its application to ion dissociation dynamics will be presented, with an emphasis placed mostly on methodology rather than on its application. Also, since general reviews on the classical trajectory method itself are available in the literature [1,70], the present review will focus on the methodology used in this laboratory which has been developed with quantitative interpretation of experimental data obtained from mass spectrometers in mind. These include the method to construct reliable global PESs using the results from ab initio calculations and the method to evaluate mode-specific energies of polyatomic products from the trajectory results. It is known that potential energy surface obtained by ab initio calculation and dynamics results calculated thereupon are not accurate enough for comparison with the experimental data. A method developed to judge and to account for such a deficiency will also be presented. Prolonged (about 10 ps or longer) calculation introduces numerically induced chaos which makes the trajectory unreliable. A convenient method

to check the advent of the numerical chaos is also presented. Numerically induced disruption of a trajectory means that the whole methodology is adequate for short time dynamics only. Hence, emphasis is placed more on the exit channel dynamics which is completed within tens of femtosecond rather than on the rate constant.

2. Construction of potential energy surface (PES)

In the conventional classical trajectory study of ion dissociation dynamics, it is essential to have a reliable global PES covering the reactant, transition state, and product regions. Trajectory results are virtually determined by PES used in the calculation. Hence, construction of accurate PES has been a subject of intense research interest.

A PES is constructed utilizing molecular information obtained from experiments and quantum chemical calculations. There are basically two different approaches to construct a PES. One is to put the global PES as a sum of many parameterized analytic functions, each of which being a potential for a particular motion such as a bond stretch [71–76,86,87]. Provisions are made such that a smooth carryover from the reactant, via transition state, to product geometries can be achieved. Parameters are fixed to fit the available molecular data. The large number of parameters involved makes this a formidable task. For example, several tens of parameters are needed to construct the PES of five- to six-atom system. Moreover, the use of pre-determined forms of potential energy functions is a needless restriction, or bias, on the shape of PES.

The second approach is to construct a PES by interpolation of molecular data such as energy and its first (gradient) and second (hessian) derivatives obtained by quantum chemical calculations at many configuration points. The Shepard interpolation method of Ischtwan and Collins [88] and the reproducing kernel Hilbert space (RKHS) method by Rabitz and coworkers [89] are the two interpolation schemes under active research. RKHS is a Hilbert space of continuous real-valued functions which possesses many useful properties for data interpolation. Several successful constructions of triatomic PES have been reported [90–94]. The Shepard interpolation scheme has been more widely applied so far. It is the main PES construction scheme incorporated in the ion dissociation dynamics package developed in this laboratory. Its essential features will be described with emphasis on those used in this laboratory.

The Shepard interpolation scheme originally proposed by Ischtwan and Collins is undergoing improvements by many research groups and various versions are available now [95–103]. In this scheme, a global PES is constructed by taking a weighted sum of local harmonic potentials at many configurations obtained by quantum chemical calculations. Namely, the potential energy $V(\boldsymbol{R})$ at configuration $\boldsymbol{R}$ is given by

$$V(\boldsymbol{R}) = \sum_k w^k(\boldsymbol{R}) V^k(\boldsymbol{R}). \quad (1)$$

Here $w^k(\boldsymbol{R})$ is the weighting function and $V^k(\boldsymbol{R})$ is the local harmonic potential in the vicinity of configuration $\boldsymbol{R}^k$.

$$V^k(\boldsymbol{R}) = V(\boldsymbol{R}^k) + \Delta^k \cdot \boldsymbol{g}_\Delta + \tfrac{1}{2}\Delta^k \cdot \boldsymbol{H}_\Delta \cdot \Delta^k. \quad (2)$$

Here $\boldsymbol{g}_\Delta$ and $\boldsymbol{H}_\Delta$ are the gradient and hessian in the coordinate system Δ which are converted from the corresponding Cartesian values evaluated in the usual quantum chemical packages. It is obvious that the method is capable of providing a faithful representation of the true PES at the quantum chemical level adopted when sufficient number of local potentials are included. The research focus here is to devise an efficient method to obtain a good representation using as small number of local potentials as possible. Some of the important aspects are as follows:

2.1. Selection of configuration points

To limit the number of local potentials used, it is necessary to identify the important points in the configuration space. For the PES used in dissociation dynamics study, the equilibrium geometries at the reactant and products and the geometry of transition

state will be such points. In addition, some points (∼40) are chosen along the minimum energy path, or the intrinsic reaction coordinate (IRC) [104,105]. A PES constructed by interpolation of local potentials at these points is called IRC-only PES.

The IRC-only PES is upgraded by adding local potentials at off-IRC points. In the upgrading scheme devised by Ischtwan and Collins, points in the configuration space which are frequently encountered in actual trajectories are selected. A number of trajectories are run on the existing PES and some, say 10, configuration points on each trajectory are sampled periodically, producing a total of N_t trajectory points denoted by $\boldsymbol{S}$. Then, the importance factor for each point is calculated by comparing with the positions (N_s in Eq. (3) denotes its number) already included in the existing PES, or database.

$$h(\boldsymbol{S}^k) = \frac{1}{N_t - 1} \frac{\sum_{n\neq k, n=1}^{N_t} v^n(\boldsymbol{S}^k)}{\sum_{i=1}^{N_s} w^i(\boldsymbol{S}^k)}, \tag{3}$$

with

$$v^n(\boldsymbol{S}^k) = \frac{1}{|\boldsymbol{T}(\boldsymbol{S}^n) - \boldsymbol{T}(\boldsymbol{S}^k)|^{2p}},$$
$$w^i(\boldsymbol{S}^k) = \frac{1}{|\boldsymbol{T}(\boldsymbol{R}^i) - \boldsymbol{T}(\boldsymbol{S}^k)|^{2p}}. \tag{4}$$

Here $2p$ is a parameter which must be equal to 2 or larger in this case to achieve convergence of the PES. It is usual to take $2p$ comparable to $3N - 6$. $\boldsymbol{T}$ is a tensor which transforms a coordinate vector into an interatomic distance vector or its inverse. The factor is large when other newly acquired trajectory points are clustered around this point and when this point is distant from the positions already included in the existing database. The point with the largest importance factor is chosen. The local potential at this point is calculated and added to the database. Other methods have been devised to select a point from N_t, such as the calculation of the variance of energy or gradient [98]. However, the quality of the global PES constructed does not seem to be very sensitive to the selection method. In the original scheme, the PES was updated until the dynamics data, such as the average kinetic energy release, obtained by trajectory calculations converged. In the method proposed by Thompson and Martinez [106] and adopted in this laboratory, energy at the selected point is obtained by ab initio calculation and also by using the current database. When the difference is larger than a preset value (typically 0.2 kcal mol^{-1}), the local potential at the new point is calculated and added to the database. The process is repeated until appropriate points can not be found any more and update fails. As a final test, energy contour diagrams are often calculated using the updated PES and compared with those obtained by ab initio scan.

2.2. Coordinate system

Since a Cartesian system shows coordinate redundancy, internal coordinate systems are more appropriate to express the PES. Even though interatomic distances were the initial choice [88], z-matrix type internal coordinates [99,102] consisting of bond length (r), bond angle (θ), and dihedral angle (ϕ) have become popular. Further improvement has been observed when the inverse bond length ($z = 1/r$) is used rather than the bond length. Also, excellent results [107] have been reported using an exponential form of bond length $e^{-\beta r}$.

Even though the construction of a global PES using one set of coordinates is desirable, it is often difficult to find a set which provides excellent representation both in the reactant and in the product regions. Then, two different sets may have to be used, one for the entrance region and the other for the exit region.

2.3. Weighting function

A local potential calculated at a configuration point included in the database is a good expression for the potential in its very vicinity. One important role of weighting function is to assure smooth carryover in a region between two database points. An excessive damping by weighting function blurs PES and makes it inaccurate even at the very vicinity of a database point. Since the quality of a global PES constructed is rather sensitive to the weighting function used, it has been the focus of active research [98,102,108,109].

A weighting function is made to have the following general property after normalization:

$$w \to \begin{cases} 0 & \text{as } |\boldsymbol{R} - \boldsymbol{R}^k| \to \infty, \\ 1 & \text{as } |\boldsymbol{R} - \boldsymbol{R}^k| \to 0. \end{cases}$$

In the Shepard interpolation [88,110,111], the weight of the kth local potential at the position $\boldsymbol{R}$ is given by

$$w^k(\boldsymbol{R}) = \frac{1}{|\boldsymbol{T}(\boldsymbol{R}) - \boldsymbol{T}(\boldsymbol{R}^k)|^{2p}}. \tag{5}$$

$\boldsymbol{T}$ is the coordinate transformation mentioned previously. Transformation to the interatomic distance vector or to its inverse is widely used, the latter being the choice in many cases. Ishida and Schatz [103] proposed to add a parameter α^2 in the denominator to remove singularity and also to have a smoothing effect at the middle of two database points. This is widely accepted now.

$$w^k(\boldsymbol{R}) = \left(\frac{1}{\alpha^2 + |\boldsymbol{T}(\boldsymbol{R}) - \boldsymbol{T}(\boldsymbol{R}^k)|^2} \right)^p. \tag{6}$$

The interatomic distances and their variants do not form a rectilinear set of coordinates. One of the results is that the same distance in Cartesian appears as different in the interatomic distance coordinate system. Such a problem is eliminated by using Cartesian distance square, δ^2, rather than $|\boldsymbol{T}(\boldsymbol{R}) - \boldsymbol{T}(\boldsymbol{R}^k)|^2$ in Eq. (5). The difficulty here is to find a common Cartesian frame in the presence of molecular rotation occurring along the trajectory [108]. A rigorous expression for δ^2 was presented by Rhee [109] as follows:

$$\delta^2 = \sum_\alpha |\boldsymbol{C}_\alpha - (\boldsymbol{\Omega}\boldsymbol{C}_\alpha^k + \boldsymbol{\tau})|^2. \tag{7}$$

Here $\boldsymbol{C}_\alpha$ and $\boldsymbol{C}_\alpha^k$ are Cartesian positions of the αth atom corresponding to $\boldsymbol{R}$ and $\boldsymbol{R}^k$, respectively. $\boldsymbol{\Omega}$ is the orthogonal rotation matrix and $\boldsymbol{\tau}$ is the translation vector. Newton's method of optimization is used to find $\boldsymbol{\Omega}$. The iterative nature of this scheme requires several times longer computing time than the previous weighting schemes.

2.4. Examples

Dissociation of CH_2OH^+ occurring via

$$CH_2OH^+ \to CHO^+ + H_2 \tag{8}$$

is a prototype ion dissociation reaction which has been investigated by several research groups over the years [71,112–119]. Fig. 1 shows a contour diagram near

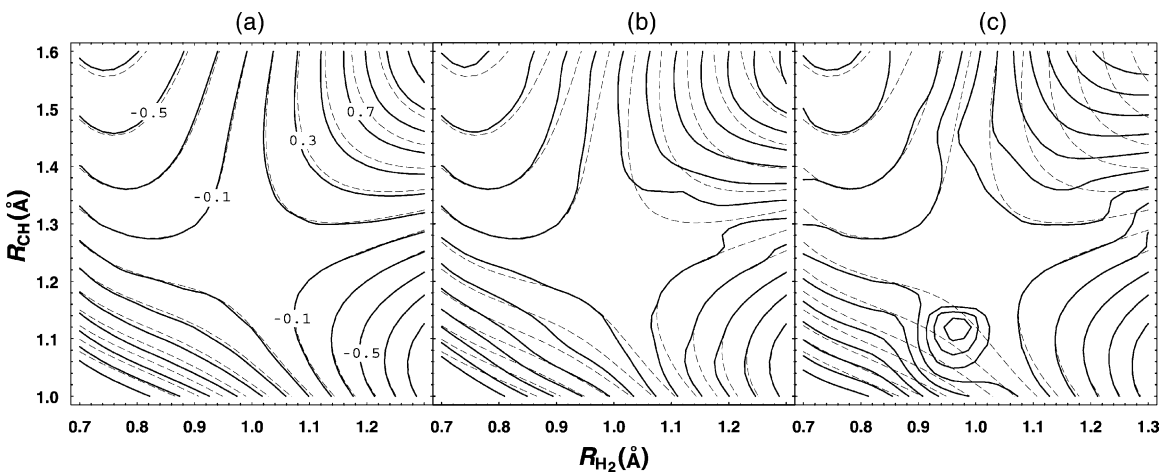

Fig. 1. Contour maps near the TS of reaction (8) for PESs constructed with (a) Cartesian weighting, (b) R-weighting, and (c) inverse R-weighting for local potentials calculated at the MP2/6-31G** level. Correct MP2/6-31G** contour obtained by ab initio scan is shown by dashed lines. The interatomic distance between two recoiling H atoms (R_{H_2}) and the distance between C and a recoiling H atom (R_{CH}) were varied while other parameters were fixed at the saddle point geometry. Energies in eV referred to the saddle point are marked. (Taken from ref. [109] with permission from AIP.)

the transition state calculated with PES constructed by interpolation as described above [109]. Ab initio calculations to obtain energy, gradient, and hessian were performed at the MP2 level using the 6-31G** basis set. The interpolation started with 40 local potentials at points on IRC and 300 potentials at off-IRC points were added by the systematic update procedure. Also shown is the PES contour at this level obtained by ab initio scan. It is seen that the PES constructed by interpolation is a good representation of the ab initio PES especially when the Cartesian weighting scheme is used.

An even more quantitative fit with the true ab initio PES is possible by adding more local potentials or by using a more elaborate scheme. For example, Fig. 2 compares the contour diagrams for the reaction

$$\mathrm{Cl} + \mathrm{H_2} \rightarrow \mathrm{HCl} + \mathrm{H} \tag{9}$$

obtained by interpolation and by ab initio scan. Ab initio calculation was done at the QCISD level with the 6-31G** basis set. Two hundred local potentials were used in the interpolation. Excellent agreement between the interpolated PES and the true ab initio PES was possible by using exponential interatomic distances ($e^{-\beta_1 r_1}$, $e^{-\beta_2 r_2}$, and $e^{-\beta_3 r_3}$) as the internal coordinates [107].

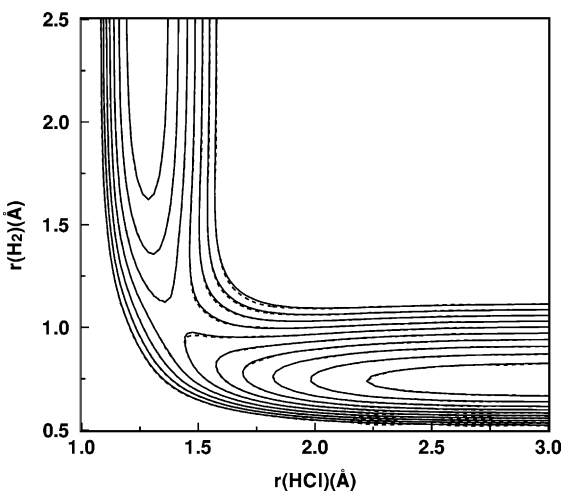

Fig. 2. The energy contour maps for the reaction (9) obtained by ab initio scan at the QCISD/6-31G** level (solid line) and by the ab initio-interpolated PES ($N = 200$, dashed line) using exponential interatomic distances as the internal coordinates. Cl–H–H bending angle was fixed at 150 degree. The spacing between the contour lines is 3.0 kcal mol^{-1} and the outermost line represents 30.0 kcal mol^{-1} with respect to the reactant energy minimum. (Taken from ref. [107] with permission from AIP.)

3. Calculation of a trajectory

Excellent reviews on the methods to calculate classical trajectory are available in the literature [1,70]. These articles and references therein are recommended for the details of the method. The essential aspects needed for actual calculation will be described here together with a brief outline of the overall method.

Calculation of a classical trajectory means evaluation of the time evolution from an initial point in the phase space by numerical integration of classical equations of motion which are usually in Hamiltonian forms.

$$\frac{\partial H}{\partial p_i} = \dot{q}_i \quad \text{and} \quad \frac{\partial H}{\partial q_i} = -\dot{p}_i. \tag{10}$$

Here q_i and p_i are the conjugate coordinate and momentum and Hamiltonian, H, is the sum of the kinetic (T) and potential (V) energies expressed in q_i's and p_i's. Expression of T is straightforward especially when Cartesian or mass-weighted Cartesian coordinate system is used. The construction of PES, V, for a system of interest was the subject of the previous section. Methods to sample a trajectory initial point and to calculate a trajectory therefrom by numerical integration of the Hamilton's equations will be described here.

3.1. Sampling

The first step in a trajectory calculation is to sample an initial point, namely position and momentum of each atom in the molecule, compatible with the experimental conditions. Sampling is done in the reactant region for the calculation of rate constant while sampling at or near the transition state is useful for the product energy partitioning calculation. Various schemes have been developed to sample initial

trajectory points [1,70,120,121]. Among these, orthant and normal mode samplings are the most widely used in reaction dynamics and will be explained here.

3.1.1. Orthant sampling

Orthant sampling was developed by Bunker and Hase [120,121] for cases where the dimension of the phase space is large and where the number of sampling is much less than the orthants in the phase space (orthants are in n-dimensional space what quadrants and octants are in two and three dimensions). It produces a microcanonical ensemble and is precise only for a collection of harmonic oscillators.

The first step in orthant sampling is to determine numerically the limits of the coordinate and momentum of each atom in the Cartesian coordinate system. Then, one unit vector with random orientation is selected and projected on the upper or lower limit of the coordinate vector to obtain the coordinate. The same is done for the momentum also. The total energy E is calculated at the phase space point sampled. Then, coordinates and momenta are scaled until E is within 0.1% of the preset energy E_0. The orthant sampling tends to provide a distribution of initial points corresponding to equipartition of internal energy among vibrational degrees of freedom. When the total energy is not far above the zero-point level, points with less than zero-point energy for some vibrational modes are frequently sampled. The problem is especially serious for high frequency vibrations.

3.1.2. Normal mode sampling [120]

Normal mode sampling avoids the above difficulty in orthant sampling by assigning the zero-point energy to each mode prior to sampling. The internal energy above the zero-point level is distributed among vibrational degrees of freedom as desired. For example, this is put in a particular mode to mimic mode-selective excitation or is distributed randomly to model a statistical situation. Then, vibrational energy in each mode is calculated. For each mode, the limits of the coordinate and momentum in the normal coordinate system are determined. For a mode with a negative eigenvalue (reaction coordinate at the saddle point), only momentum limits are determined. A random number R ($0 \leq R \leq 1$) is selected. By multiplying R to the upper or lower limit of the coordinate, displacement in a normal coordinate is obtained. Sampling of the momentum is similar but uses $\sqrt{1-R^2}$. The total energy E is calculated and compared with the preset energy E_0. The coordinate is scaled until E is within 0.1% of E_0.

3.2. Numerical integration

A trajectory starting from an initial point in the phase space is calculated by numerical integration of Hamilton's equations. In the rate constant calculation, a trajectory is terminated some time after the system has crossed the transition state and entered the product region. In the product energy partitioning calculation, termination is done when the dissociation is complete (when the center of mass distance between the fragments is larger than a cutoff value) or when the system relaxes toward the reactant. The energy conservation error, $|\Delta E|/E$, is monitored to check the integration accuracy. The time step of integration may have to be reduced to keep this within the preset value (10^{-6}, for example). Some important integrators are as follows [122–124].

3.2.1. The fourth order Runge–Kutta integrator (RK4)

The Runge–Kutta method is a single-step method which uses the position and momentum at $t = t_0$ to find those at $t = t_0 + h$. Even though the Taylor expansion up to the fourth order is taken into account in RK4, costly calculation of the second and higher order terms are avoided by including data at three estimated points between t_0 and $t_0 + h$. RK4 is self-starting, stable, and accurate. The main disadvantage is that it does not provide an estimate of accuracy, which must be checked indirectly, for example, by calculating the energy conservation error.

3.2.2. Adams–Moulton integrator (AM)

The Adams–Moulton method is a multi-step method which uses the position and momentum at $t = t_0$ and

at some previous points to find those at $t = t_0 + h$. AM can be run with variable time step within the preset integration accuracy. AM is fast and accurate, more so than RK4, and is the integrator of choice in this laboratory. Since AM is not self-starting, RK4 is run at several points near the initial point. AM is often combined with the Adams–Bashforth technique, which results in predictor–corrector methods.

We also tested Gear's integrator which belongs to a family of backward differentiation formulas and Verlet and velocity-Verlet integrators which are widely used in the molecular dynamics simulation. The former is known to be appropriate to handle stiff problems. The Verlet-type integrators are simple, fast, and display decent energy conservation even after long term integration. However, we found [125] that trajectory equivalence (to be explained in a following section) decayed very rapidly with these integrators. Hence, even though RK4 and AM integrators are known to accumulate errors, these have been found to be more appropriate for the calculation of trajectories in the short term.

4. Rate constant and product energy partitioning

4.1. Rate constant

To calculate a rate constant a number of trajectories, N_0, are run starting from initial points sampled to be compatible with the system of interest. Calculation of a trajectory is terminated when reaction has occurred, for example, as judged from the distance between the two fragments. The number of unreactive trajectories, N, remaining after time t is counted. Rate constant k is determined as the slope of the semilog plot of N vs. t [70].

$$N = N_0 \, \mathrm{e}^{-kt}. \tag{11}$$

4.2. Relative translational energy

The relative translational energy for the unimolecular dissociation reaction A → B + C is calculated from a trajectory result as [70]

$$E_\mathrm{t} = \tfrac{1}{2}\mu \boldsymbol{v}_\mathrm{rel}^2. \tag{12}$$

Here $\boldsymbol{v}_\mathrm{rel} = \boldsymbol{v}_\mathrm{B} - \boldsymbol{v}_\mathrm{C}$ and μ is the reduced mass of the B–C system.

4.3. Rotational energy

The rotational energy of a diatomic or asymmetrical polyatomic product can be calculated from a trajectory result as [70]

$$E_\mathrm{r} = \tfrac{1}{2}\boldsymbol{\omega} \cdot \boldsymbol{J}. \tag{13}$$

Here $\boldsymbol{\omega}$ is the angular velocity and $\boldsymbol{J}$ is the angular momentum. The rotational analysis for linear and symmetric top products is not straightforward due to the complication arising from vibration–rotation interaction. Recently, a good approximate treatment of linear triatomic case was developed [126]. Let us designate A, B, and C as the three rotational axes, A being the figure axis in the equilibrium geometry. Defining a two-dimensional angular momentum perpendicular to A as

$$\boldsymbol{J}^{2\mathrm{D}} = \boldsymbol{J}_\mathrm{B} + \boldsymbol{J}_\mathrm{C} = \boldsymbol{J} - \boldsymbol{J}_\mathrm{A}, \tag{14}$$

it was found that the two-dimensional angular velocity, $\boldsymbol{\omega}^{2\mathrm{D}}$, was an excellent approximation for the pure rotational angular velocity.

$$\boldsymbol{\omega}^{2\mathrm{D}} = \boldsymbol{I}^{-1} \cdot \boldsymbol{J}^{2\mathrm{D}}. \tag{15}$$

The rotational energy under this approximation is simply given by

$$E_\mathrm{r} = \tfrac{1}{2}\boldsymbol{\omega}^{2\mathrm{D}} \cdot \boldsymbol{I} \cdot \boldsymbol{\omega}^{2\mathrm{D}}. \tag{16}$$

4.4. Mode-specific vibrational energy

Until recently, accurate calculation of mode-specific vibrational energy of a polyatomic product from a trajectory result was a very difficult job. In many trajectory studies involving polyatomic products, E_t and E_r were subtracted from the total energy and the remainder was presented as the total vibrational energy. One way to separate this into each normal

mode is to use Cartesian eigenvector and obtain the displacement (Q_l) and velocity ($\dot{Q}_l$) along each normal mode (l). Then, kinetic (T) and potential (V) parts of the energy of this mode are given by [127,128]

$$T_{\mathrm{v},l} = \tfrac{1}{2}\dot{Q}_l^2, \qquad V_{\mathrm{v},l} = \tfrac{1}{2}\lambda_l^2 Q_l^2. \tag{17}$$

Here λ_l is the force constant of the lth mode. Calculation of a mode energy using Eq. (17) results in a significant error as will be shown later.

The main problem associated with the use of Cartesian eigenvectors arises from the fact that these are correct only at the equilibrium geometry and hence are not adequate for large amplitude motions. Such a problem can be made less serious by expressing the normal mode eigenvectors in terms of a set of internal coordinate vectors which lie more or less along the vibrational motions even at large displacements [129]. For example, eigenvectors of H_2O expressed in r_1, r_2, and θ coordinates are more adequate than the usual Cartesian forms. The formalism to evaluate mode-specific vibrational energy from a trajectory result using internal eigenvectors is rather complicated. Therefore, only a brief outline will be presented.

The Cartesian velocity is divided into two; $\boldsymbol{v}$ is the velocity free of angular motion and $\boldsymbol{u}$ is that of angular motion. $\boldsymbol{v}$ is converted to the velocity in an internal coordinate system, $\dot{\boldsymbol{s}}$, as follows:

$$\dot{\boldsymbol{s}} = \boldsymbol{B} \cdot \boldsymbol{M}^{-1/2} \cdot \boldsymbol{v}. \tag{18}$$

Here $\boldsymbol{B}$ is the usual $\boldsymbol{B}$-matrix in the vibrational problem and $\boldsymbol{M}$ is the diagonal matrix of atomic masses. $\dot{\boldsymbol{s}}$ is further transformed to the mass-free velocity using the $\boldsymbol{G}$-matrix ($\boldsymbol{G} = \boldsymbol{B}\boldsymbol{M}^{-1}\boldsymbol{B}^{\mathrm{T}}$).

$$\boldsymbol{V}_s = \boldsymbol{G}^{-1/2} \cdot \dot{\boldsymbol{s}}. \tag{19}$$

Then the kinetic energy of the lth mode is given by

$$T_{\mathrm{v},l} = \tfrac{1}{2}[(\boldsymbol{\Lambda}_l \cdot \boldsymbol{V}_s)^2 + (\boldsymbol{L}_l \cdot \boldsymbol{u})^2]. \tag{20}$$

Here $\boldsymbol{\Lambda}_l$ and $\boldsymbol{L}_l$ are the eigenvectors of the lth mode expressed in the internal and Cartesian coordinate systems, respectively. To evaluate the potential part, displacement along the lth normal coordinate is calculated from a trajectory result as follows:

$$S_l = \boldsymbol{\Lambda}_l \cdot \boldsymbol{G}_0^{-1/2} \cdot (\boldsymbol{s} - \boldsymbol{s}_0). \tag{21}$$

Here $\boldsymbol{s}_0$ is the equilibrium geometry and $\boldsymbol{G}_0$ is the $\boldsymbol{G}$-matrix calculated at this geometry. In a scheme called the elimination method, the potential of the lth mode is calculated with the displacements of other modes ignored.

$$V_{\mathrm{v},l} = V(\boldsymbol{s}_0 + S_l \boldsymbol{G}_0^{1/2} \cdot \boldsymbol{\Lambda}_l) - V(\boldsymbol{s}_0). \tag{22}$$

It is to be mentioned that the mechanical anharmonicity is accounted for in this formula. The remaining source of error in mode-specific energy assignment is the mode–mode coupling. A simple way to correct for this error is to calculate potential energy, $V_{\mathrm{v},lm}$, for simultaneous displacements along the lth and mth modes and compare with $V_{\mathrm{v},l} + V_{\mathrm{v},m}$. Since difference between these values must arise due to mode–mode coupling, the difference is divided evenly to the lth and mth mode.

4.5. Example

Various methods to calculate the mode-specific energies were tested in ref. [129] with two nonreacting triatomic systems H_2O and HCN and with CHO^+ which is the product of reaction (8). The PESs constructed by interpolation of local potentials obtained at the MP2/6-31G** level were used. Rotational energies were added in all the cases. More than 1000 trajectories were run for each system. At a trajectory end point, the rotational energy (E_{r}) and the Coriolis energy (E_{Cori}) were calculated, which were small fractions of the total internal energy. Five different schemes to evaluate the energy of the ith vibrational mode, E_{v}^i, were tested. The results from three schemes will be presented here, which are the most representative. These are (I) use of Cartesian eigenvectors and harmonic approximation for vibration (Eq. (17)), (II) use of internal eigenvectors and harmonic approximation, and (III) use of internal eigenvectors and the elimination method (Eqs. (20) and (22)). The total internal energies were calculated by summing all the

Table 1
Vibrational energies (in eV) of each normal mode evaluated by schemes I–III, and the errors (δ in %, Eq. (23)) in the mode-specific analysis for nonreacting systems H_2O and HCN and for CHO^+ generated by reaction (8)[a]

	Scheme I (Cartesian/harmonic)	Scheme II (internal/harmonic)	Scheme III (internal/elimination)
H_2O			
ν_1[b]	0.60 ± 0.75	0.45 ± 0.30	0.42 ± 0.26
ν_2[b]	0.30 ± 0.28	0.30 ± 0.28	0.29 ± 0.27
ν_3[b]	0.35 ± 0.34	0.31 ± 0.28	0.31 ± 0.28
δ (%)	24.1 ± 75.9	5.9 ± 16.6	3.0 ± 10.0
HCN			
ν_1	0.28 ± 0.26	0.28 ± 0.27	0.27 ± 0.23
ν_2	0.39 ± 0.21	0.45 ± 0.25	0.45 ± 0.26
ν_3	0.87 ± 0.76	0.29 ± 0.25	0.28 ± 0.23
δ (%)	52.1 ± 71.0	1.1 ± 10.8	0.0 ± 3.5
CHO^+			
ν_1	0.34 ± 0.24	0.25 ± 0.20	0.27 ± 0.22
ν_2	0.36 ± 0.17	0.39 ± 0.19	0.41 ± 0.20
ν_3	0.35 ± 0.35	0.12 ± 0.13	0.13 ± 0.13
δ (%)	23.5 ± 33.5	-7.0 ± 4.9	0.0 ± 4.1

Taken from ref. [129] with permission from AIP.
[a] Correct total vibrational energies are obtained by subtracting translational and rotational energies from the total energy.
[b] ν_1, ν_2, and ν_3 are the symmetric stretching, bending, and asymmetric stretching modes, respectively.

mode-specific energies. These were compared with the correct values (E_{in}) to estimate the relative errors (δ) as follows (Table 1):

$$\delta = \frac{\left(\sum_i E_v^i + E_r + E_{Cori}\right) - E_{in}}{E_{in}}. \quad (23)$$

Scheme I was found quite inaccurate with the average errors of 24, 52, and 24% for H_2O, HCN, and CHO^+, respectively. Use of the internal eigenvectors in scheme II substantially reduced the errors to 6, 1, and −7%, respectively. Finally, accounting for the mechanical anharmonicity in scheme III further reduced the error to a negligible level, 3, 0, and 0%, respectively. Scheme III was tested for other systems including a four-atom product and satisfactory results were reported [119,130–132].

5. Scaling of trajectory results

As mentioned earlier, trajectory results are essentially determined by the PES used in the calculation. The method to construct PES by interpolation of local potentials obtained by quantum chemical calculation is systematic, unbiased, and attempts to produce a PES which is a good representation of a quantum chemical PES. The problem here is that the quantum chemical PES itself may not be a good representation of the real PES. One may attempt to alleviate such a difficulty by adopting a higher quantum chemical level. Still, some difficulties are encountered. The first difficulty is that an efficient software to calculate the hessian, which is needed to obtain a local potential, is implemented at moderately high ab initio levels only in commercial quantum chemistry packages. The second difficulty, which is also a practical one, is that even though raising the quantum chemical level is known to improve the accuracy, the improvement achieved is not quite significant compared to tremendous computing time further needed. The third is that even with the use of the highest level accessible, there is no guarantee that PES at this level is a good representation of the real one. Hence, a method is needed to obtain reliable results from trajectory calculations on PES constructed at a moderately high quantum chemical level and to assure their reliability. The

scaling theorem for classical trajectory was found in this laboratory and used to handle the above issues.

5.1. Scaling relation for dynamical properties

When two PESs are qualitatively similar even though not quantitatively, trajectory results on these surfaces are expected to be similar. The scaling relation between the trajectory results on exactly scalable PESs was derived, which is called the scaling theorem [119,132].

Let us consider two PESs related by simple scaling:

$$V_s(\boldsymbol{q}_s) = s^2 V(\boldsymbol{q}). \tag{24}$$

Two-phase space points, one on each surface, is called equivalent when the following conditions are met for the positions and momenta:

$$\boldsymbol{q}_s = \boldsymbol{q}, \qquad \boldsymbol{p}_s = s \cdot \boldsymbol{p}. \tag{25}$$

Eq. (25) assures simple scaling similar to Eq. (24) for the kinetic energy, and hence the total energy also.

$$E_s(\boldsymbol{q}_s, \boldsymbol{p}_s) = s^2 E(\boldsymbol{q}, \boldsymbol{p}). \tag{26}$$

For trajectories initiated from equivalent points, it can be shown that the equivalence is maintained throughout the trajectories when phase space points at scaled times are compared [119].

$$t_s = s^{-1} t. \tag{27}$$

This scaling theorem leads to important relations between dynamic properties obtained on PESs related by simple scaling. The fact that the trajectories initiated from the equivalent phase space points terminate at equivalent points means that the mode-specific energies [129] are also scaled by the same factor s^2. For reactive trajectories, it can be shown that the rotational and translational energies of products are similarly scaled also [119]. Scaling theorem also leads to simple relation between rate constants evaluated on simply scaled PESs. The scaling relation between rate constants for unimolecular reaction can be easily derived based on the usual relation.

$$N = N_0 \, \mathrm{e}^{-kt}, \qquad N_s = N_0 \, \mathrm{e}^{-k_s t}. \tag{28}$$

Since the number of unreactive trajectories at the equivalent time (Eq. (27)) is the same, the following relation is obtained [132]:

$$k_s = s \cdot k. \tag{29}$$

The same relation holds for the rate constants of bimolecular reactions also [132]. The validity of this relation was also checked for the RRKM–QET rate constant [132], and the relation was found to be valid in the classical limit in this case. Derivation of the relation is based on classical mechanics and hence is not adequate to handle quantum effects such as tunneling and the zero-point effect. Namely, the relation does not hold rigorously for reactions occurring below or a little above the reaction barrier. Practical utility of the scaling relation is as follows. We suppose that a PES constructed at a quantum chemical level is qualitatively similar, or nearly scalable, to the real one, even though height of the barrier is somewhat different. Then the scaling theorem suggests that a decent estimation of dynamics data can be obtained by carrying out trajectory calculations on the quantum chemical PES and scaling the results. A question here is whether a quantum chemical PES would be qualitatively similar to the real one. An answer to this question is difficult, or impossible, to find because there is no way to determine a real PES. Approach taken in this laboratory is to construct quantum chemical PESs at successively higher levels and observe their convergence.

5.2. Similarity factors

To test the proposition that dynamics results on qualitatively similar PESs be scalable, one needs a definition for qualitative similarity of PESs and also for similarity of dynamics results on these surfaces.

To be rigorous, the similarity of two PESs must be considered over the entire configuration space. To simplify the matters, a definition of PES similarity was proposed which took into account the geometrical variation along the intrinsic reaction coordinate only [119]. To treat the exit channel problem, the energy along IRC in each PES was normalized to the

reverse barrier. The normalized potential energy was called ϵ. Many points along the exit channel IRC were sampled at equal energy interval, with ϵ_i denoting the normalized energy at the point i. Normalized difference between the interatomic distance vectors at the points i and $i+1$ was defined as $\boldsymbol{D}_i$. Then, similarity of a PES A to the reference PES R was defined as

$$S_{\mathrm{P}}^{\mathrm{A}} = \frac{\sum_i \epsilon_i (\boldsymbol{D}_i^{\mathrm{A}} \cdot \boldsymbol{D}_i^{\mathrm{R}})}{\sum_i \epsilon_i}. \tag{30}$$

When PES A is simply scaled to R, S_{P} is 1. Otherwise, S_{P} becomes smaller than 1.

To test whether trajectory studies on qualitatively similar PESs would result in similar dynamics data, a measure of similarity between dynamics data obtained on A and R surfaces is needed. Dynamics similarity factor for the exit channel problem was defined as follows:

$$S_{\mathrm{D}}^{\mathrm{A}} = 1 - \left[\sum_i (f_i^{\mathrm{A}} - f_i^{\mathrm{R}})^2 \right]^{1/2}. \tag{31}$$

Here f_i is the normalized energy of the ith degree of freedom, either translational, rotational, or vibrational, of the products. Here again, S_{D} is 1 when energy partitioning data from the A and R surfaces are exactly scaled. Otherwise S_{D} becomes smaller than 1. Utility of the S_{P} factor is as follows. We calculate the potential energy diagram along IRC at successively higher ab initio levels. Taking the one obtained at the highest level as the reference, S_{P} factors for lower levels are calculated. When these converge to 1 as the levels get higher, we take the highest level adopted as a good representation for the real system, construct PES at this level, and carry out dynamics study. This strategy is based on the assumption that the energy partitioning data converge ($S_{\mathrm{D}} \rightarrow 1$) as the convergence of PES shape ($S_{\mathrm{P}} \rightarrow 1$) is achieved at high ab initio level. This was tested and some results are presented below.

5.3. Example 1: Scaling of the product mode-specific energy

To investigate the convergence of the product mode-specific energy, the PESs for the following reaction were constructed at various quantum chemical levels, including semi-empirical, ab initio, and density functional theory levels.

$$CD_2OH^+ \rightarrow CDO^+ + HD. \tag{32}$$

A PES obtained at the QCISD level was taken as the reference and the S_{P} factors for other levels were calculated. The results are shown in Table 2. Three thousand trajectories were run on PES at each level. The normalized mode-specific energies calculated from the trajectory results are shown in Table 2 also. It is seen that dynamics data obtained on semi-empirical surfaces are noticeably different from those on the reference surface. It is to be noted that these surfaces do not quite resemble the QCISD surface as evidenced by small S_{P} factors. As the level goes up, the normalized dynamics data become similar to those on the reference. The trend becomes more clear in Fig. 3 which shows a strong positive correlation between S_{P} and S_{D} factors. Also important is the fact that dynamics data obtained at moderate and moderately high quantum chemical levels are similar, or have

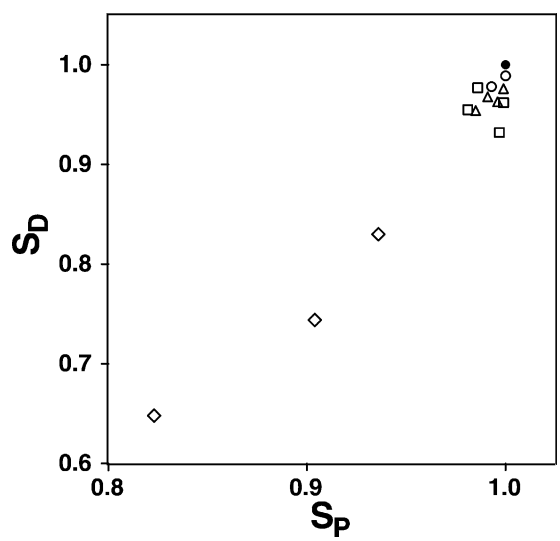

Fig. 3. Correlation between the dynamical (S_{D}, Eq. (31)) and PES (S_{P}, Eq. (30)) similarity factors for reaction (32). QCISD/6-31G** level was used as the reference. Semi-empirical (◇), HF (△), MP (○), QCISD (●), and DFT (□) results. (Taken from ref. [119] with permission from AIP.)

Table 2
Product mode-specific energies of the reaction (32) normalized to the reverse barrier (in %) calculated using PESs constructed at various quantum chemical levels, the dynamics similarity factors (S_D, Eq. (31)) calculated therefrom, and the PES similarity factors (S_P, Eq. (30))

Level	E_t	E_r (HD)	E_v (HD)	E_r (CDO^+)	E_v (CDO^+)			S_D	S_P
					ν_1[a]	ν_2[a]	ν_3[a]		
MNDO	50.9	20.3	7.8	1.4	3.8	14.1	1.3	0.744	0.904
AM1	41.2	14.4	18.2	1.9	7.6	13.9	2.0	0.648	0.823
PM3	56.9	8.5	9.3	2.3	1.5	14.8	4.5	0.830	0.936
3-21G**	69.3	6.9	5.4	1.2	6.2	10.7	1.3	0.954	0.985
4-31G**	73.3	4.3	5.1	1.5	3.5	12.5	1.1	0.968	0.991
6-31G*	69.8	6.4	6.5	1.3	4.0	12.5	1.4	0.963	0.996
6-31G**[b]	72.4	5.2	5.0	1.7	3.1	12.7	1.0	0.976	0.999
MP2	73.3	6.5	3.8	1.3	4.1	10.7	0.9	0.978	0.993
MP4 (SDQ)	72.3	7.3	4.1	1.4	3.4	11.4	1.0	0.989	1.000
QCISD[c]	72.5	7.0	4.9	1.5	2.7	11.3	0.9	1.000	1.000
BLYP	68.6	7.9	6.7	1.5	2.7	10.4	1.7	0.955	0.981
BP86	66.9	10.7	5.4	1.8	2.6	11.4	1.5	0.932	0.997
B3LYP	70.8	8.3	5.0	1.7	2.1	10.9	1.4	0.977	0.986
B3PW91	70.7	10.1	4.4	1.9	1.7	11.4	1.3	0.962	0.999

Taken from ref. [119] with permission from AIP.
[a] ν_1, ν_2, and ν_3 are the symmetric stretching, bending, and anti-symmetric stretching vibrations of CDO^+, respectively.
[b] 6-31G** basis set was used in the calculations at the post-SCF and DFT levels.
[c] QCISD results were taken as the reference in the calculation of similarity factors.

converged. This suggests that the energy partitioning data calculated at the moderately high levels of theory such as QCISD/6-31G** or MP4 (SDQ)/6-31G** would be reliable. Survey of the data in Table 2 suggests that dynamics results on PESs constructed at even higher levels would not be significantly different from those at the moderately high levels, or the trajectory results have converged.

Scaling of product energy partitioning was also tested for the following neutral reaction [130]:

$$H_2CO \rightarrow H_2 + CO. \quad (33)$$

This reaction was chosen because the experimental distribution of translational, rotational, and vibrational energies of products are known [133–136]. The PESs were constructed with coordinates appropriate for the product region at the HF, MP2, QCISD, and B3LYP levels of theory using the 6-31G** basis set. The reverse barriers calculated at these levels are 106.58, 94.16, 93.26, and 79.52 kcal mol^{-1}, respectively, compared to 77.97 kcal mol^{-1} estimated in the experiment. These data were used to estimate the scaling factors (s^2) which, in turn, were used to scale the trajectory results. The scaled kinetic energy release distribution and the distributions of the product vibrational and rotational quantum numbers calculated at these levels are shown in Figs. 4–7. It is to be noted that the scaled

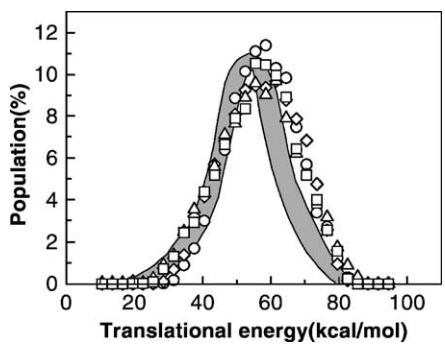

Fig. 4. The scaled translational energy (in kcal mol^{-1}) distributions obtained on PESs constructed at HF (○), MP2 (◇), QCISD (□), and B3LYP (△) levels for reaction (33). The shaded area is the range for acceptable fit to experimental data as reported by Moore and coworkers [133]. (Taken from ref. [130] with permission from AIP.)

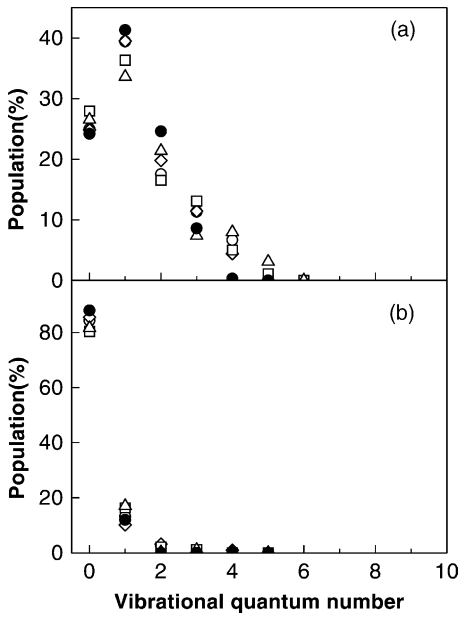

Fig. 5. The vibrational populations of (a) H_2 and (b) CO, which are the products of reaction (33). Calculations at the level of HF (○), MP2 (◇), QCISD (□), and B3LYP (△) levels, and the experimental data (●). (Taken from ref. [130] with permission from AIP.)

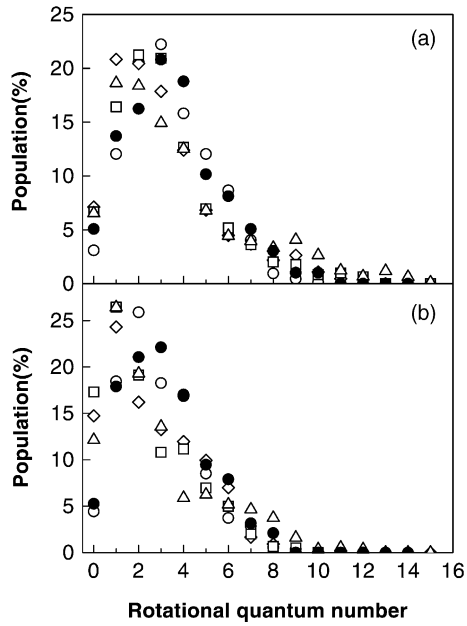

Fig. 6. Rotational populations of product H_2 of reaction (33) in (a) $v = 1$ and (b) $v = 3$ vibrational states. HF (○), MP2 (◇), QCISD (□), and B3LYP (△) levels, and the experimental data (●). (Taken from ref. [130] with permission from AIP.)

mode-specific energies calculated are in excellent, or nearly quantitative, agreement with the experimental data. This demonstrates that the difficulty in the trajectory approach arising from inaccurate energetic data obtained at moderately high quantum chemical levels can be overcome, at least partially, by utilizing the scaling relation.

5.4. Example 2: Scaling of the rate constant

Scaling relation for the rate constant was numerically checked for the reaction (33) [132]. A global PES was constructed at the HF/6-31G** level using coordinates appropriate in the reactant region. The classical forward barrier calculated at this level was 104.6 kcal mol^{-1}. This PES was scaled with the scaling factors (s^2) of 0.25 and 4 with the corresponding forward barriers of 26.15 and 418.4 kcal mol^{-1}. A total of 1050 trajectories were run on each surfaces ($s = 0.5$, 1, and 2) with the scaled internal energies of 35.0, 140.0, and 560.0 kcal mol^{-1}, respectively. The rate constants calculated by the semilog plots in Fig. 8 were 0.89×10^{11}, 1.78×10^{11}, and 3.56×10^{11} s^{-1}. $k_{s=0.5}$:$k_{s=1}$:$k_{s=2}$ ratio of 0.5:1:2 is exactly as expected from Eq. (29). This confirms the validity of the rate constant scaling relation, Eq. (29).

The RRKM rate–energy data for the same reaction were also calculated using the molecular parameters obtained at the HF/6-31G** level with the scaling factors (s^2) of 1.0, 1.44, and 4.0, Fig. 9(a). It is to be noted that the rate constant at a particular internal energy changes dramatically with the scaling factor used. These data were converted to the scaled forms by invoking the scaling relations for the internal energy (Eq. (26)) and rate constant (Eq. (29)). The rate–energy data calculated using widely different forward barriers, 26.16–418.4 kcal mol^{-1}, nearly overlap after scaling except at very near the reaction threshold where the zero-point energy effect in the RRKM calculation must be especially prominent, Fig. 9(b). This demonstrates that a good estimate of RRKM rate constant can be made by calculating

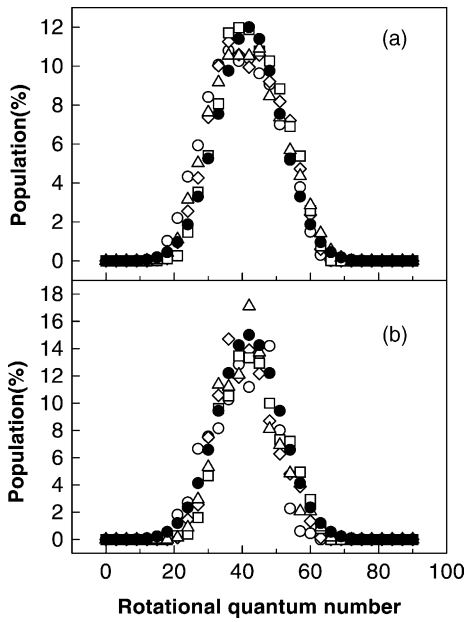

Fig. 7. Rotational populations of product CO of reaction (33) in (a) $v = 0$ and (b) $v = 1$ vibrational states. HF (○), MP2 (◇), QCISD (□), and B3LYP (△) levels, and the experimental data (●). (Taken from ref. [130] with permission from AIP.)

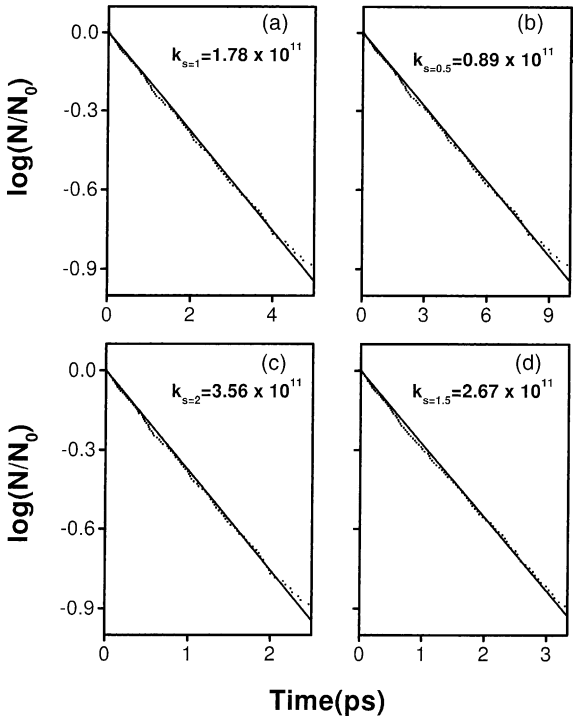

Fig. 8. The semilog plots (···) of the fractions (N/N_0) of the unreactive trajectories vs. time for reaction (33). (a) The trajectories on the interpolated PES constructed at the HF/6-31G** level. The same surface was scaled to obtain the other results. The s factors used were (b) 0.5, (c) 2, and (d) 1.5. Scaled internal energies were also used, (a) 140.0, (b) 35.0, (c) 560.0, and (d) 315.0 kcal mol^{-1}. Lines (—) are the least squres fits to Eq. (28). The rate constants evaluated with the slopes of the lines are indicated. (Taken from ref. [132] with permission from AIP.)

with molecular parameters obtained at moderately high quantum chemical level and scaling the results with the experimental forward barrier information. Theoretical RRKM rate–energy data for this reaction were reported by Miller [137] and also by Troe [138]. The forward barriers used in the calculation were 93.6 and 88.5 kcal mol^{-1}, respectively. With the forward barrier of 104.6 kcal mol^{-1} at the HF level, the scaling factors for the PESs used by the above investigators become 0.895 and 0.846, respectively. The rate–energy data reported by the above investigators were scaled accordingly and are compared with the HF/6-31G** result in Fig. 10. The excellent agreement among these data clearly demonstrates utility of the scaling relation for rate constant estimation.

6. Numerically induced chaos

Reaction systems we are interested in are inherently nonlinear. In such cases, it is well known that even a tiny effect can vary the conditions such that the future outcome is entirely different from what might have been expected [139]. In the present case, factors affecting a trajectory can creep in at various stages, for example, at the time of PES construction, initial state sampling, etc. Advent of chaos in the time evolution of a nonlinear system has been a subject of great interest [140–143]. However, not much attention has been paid to this effect in the field of computational reaction dynamics partly because the usual approach here is to evaluate dynamics properties as averages of results from many trajectories. It is certain that the effect of chaos can not be ignored when one attempts to gain physical information from a single, or limited number

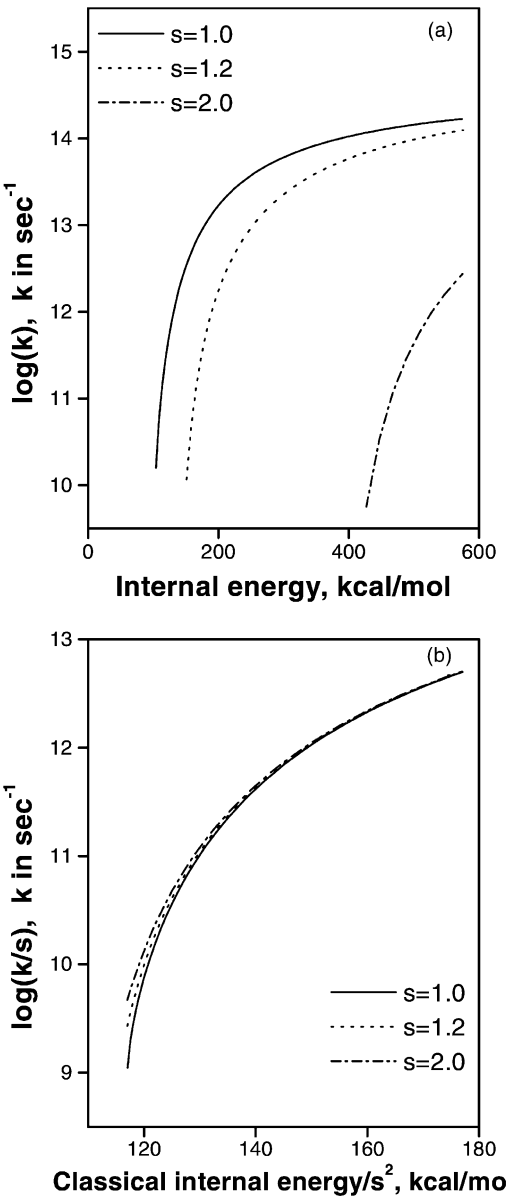

Fig. 9. (a) The RRKM rate–energy relations for reaction (33). The solid curve (—) was calculated with HF/6-31G** data. The dots (···) and dash-dots (–·–·–) were obtained using parameters scaled with the s factor of 1.2 and 2.0, respectively. (b) The scaled RRKM rate–energy relations for reaction (33) obtained by transforming the data in (a). The abscissa is the classical internal energy referred to the reactant energy minimum divided by s^2. The ordinate is the logarithm of the rate constant divided by s. The solid curve (—), dots (···), and dash-dots (–·–·–) represent the results for $s = 1$, 1.2, and 2.0, respectively. (Taken from ref. [132] with permission from AIP.)

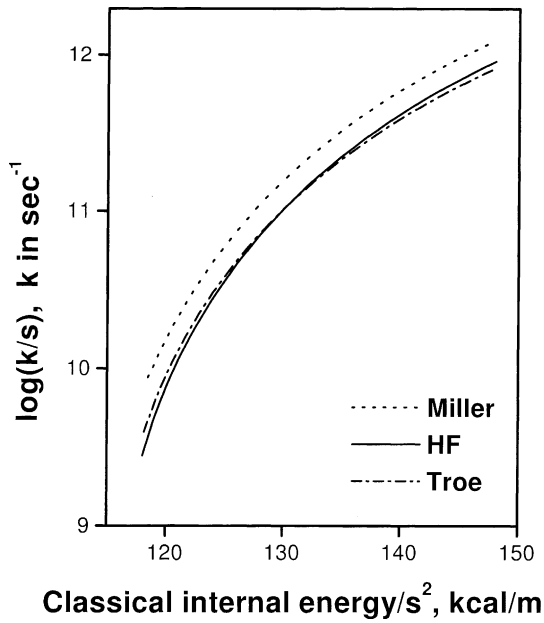

Fig. 10. The scaled RRKM rate–energy relations for reaction (33) obtained using Miller's (···) and Troe's (–·–·–) parameters are compared with the HF/6-31G** result (—). The formers were scaled using the scaling factors (s^2) of 0.895 and 0.846, respectively. (Taken from ref. [132] with permission from AIP.)

of, trajectory. The chaos we are interested in here is the one inherent in computation with digital computers.

In numerically solving equations of motion, two kinds of numerical errors are involved, truncation and round-off errors. Truncation error which is caused by truncation of infinite Taylor series can be kept small by choosing a proper integrator and by using a small time step. It is possible to get some idea on its influence by calculating the energy conservation error. Round-off error is due to the finite precision arithmetic used in a computer. Its influence increases as the total number of integration steps increases and prevents one from using a very small time step. It is well known that tiny round-off error can accumulate rapidly and alter the course of a trajectory significantly even when the energy conservation error is negligible [144,145]. Influence of the numerical chaos originating from the round-off error may be simply checked by changing the arithmetic precision adopted in computation. However, tremendous amount of

computation time is often needed for such an effort and the outcome can be indecisive.

An easy way to check the advent of chaos, we found, is to calculate equivalent trajectories and inspect differences in their time evolutions [125]. In the previous section, it was shown that the rate constants of reaction (33) obtained from three sets of equivalent trajectory calculations using $s^2 = 1$, 2^{-2}, and 2^2 were exactly scaled as dictated by Eq. (29). Namely no evidence for the influence of numerically induced chaos was seen. When a similar calculation was done with $s = 3/2$ (results shown in Fig. 8(d)), the rate constant scaling was found to hold not exactly but only up to the third significant digit. Then, it was realized that rigorous rate constant scaling for $s^2 = 1$, 2^{-2}, and 2^2 was due to binary nature of digital computation.

The method devised to check the advent of numerically induced chaos is as follows. After constructing a PES, one prepares a simply scaled PES using a scaling factor (s^2) other that 2^{2n} (n is an integer). Two trajectories, one on each PES, are run initiated from equivalent phase space points. Then, equivalence of two trajectories are checked at equivalent times by calculating

$$E_q = \frac{|\boldsymbol{q}_1 - \boldsymbol{q}_s|}{|\boldsymbol{q}_1|} \quad \text{or} \quad \frac{|\boldsymbol{p}_1 - \boldsymbol{p}_s/s|}{|\boldsymbol{p}_1|}. \tag{34}$$

Here $\boldsymbol{q}_1$ and $\boldsymbol{p}_1$ are the atomic positions and momenta at a point on the original trajectory and $\boldsymbol{q}_s$ and $\boldsymbol{p}_s$ are those on the scaled one. $E_q = 0$ when equivalence is strictly maintained. As time elapses and the effect of round-off error accumulates, E_q increases and eventually approaches 1 indicating complete breakup of equivalence. Using double precision arithmetic, it takes only several picoseconds for complete breakup of equivalence as will be seen in the following example. Use of extended double precision helps, but only slightly. This is the reason why use of computational dynamics must be limited to fast processes such as the rate constant calculation for a reaction occurring on a picosecond or shorter time scale and calculation of product energy partitioning. One may attempt the rate constant calculation for a reaction occurring on a longer time scale and obtain results indicating statistical nature of the reaction. One can not be sure in this case, however, whether the statistical behavior observed is due to the inherent vibrational ergodicity (rapid intramolecular vibrational redistribution (IVR)) of the system or is caused by scrambling arising from the numerically induced chaos. Computational dynamics has been widely used to study IVR occurring in polyatomic systems [146–151]. A generally accepted view on this phenomenon is that IVR is complete within several picoseconds in most of the cases. Considering that breakup of equivalence caused by numerical chaos is completed within the same time scale, a special caution is called for in such studies.

6.1. *Example: Intramolecular dynamics of* HOD

To study the breakup of equivalence caused by numerical chaos, intramolecular dynamics of HOD was calculated using the following potential energy [125]:

$$V = \tfrac{1}{2}h_{11}z_1^2 + \tfrac{1}{2}h_{22}z_2^2 + \tfrac{1}{2}h_{33}\theta^2 + h_{12}z_1z_2 + h_{13}z_1\theta + h_{23}z_2\theta. \tag{35}$$

Here z_1 and z_2 are the reciprocal displacements of the OH and OD bond lengths, respectively, θ is the bond angle displacement, and h_{ij}'s are the components of the hessian matrix. h_{ij}'s calculated at the

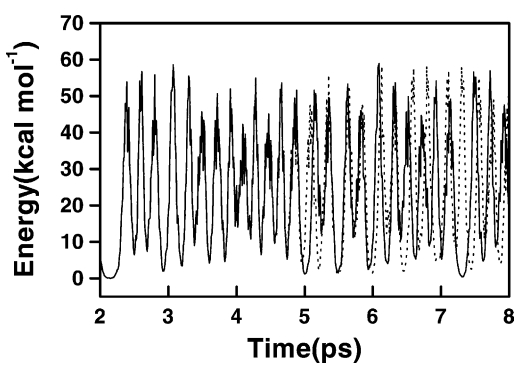

Fig. 11. Time evolution for the bending mode energy of HOD initiated at the bending phase angle of 229.15° and the bending energy of 60 kcal mol^{-1} is shown as the solid line (—). The model potential, Eq. (35), is used. The dashed line (– – –) is the result from the scaled calculation ($s = 3$). (Taken from ref. [125] with permission from Elsevier.)

MP2/6-31G** level were used. Even though only quadratic terms are present in the above formula, vibrational modes are still coupled through the kinetic term in the Hamiltonian.

Fig. 11 shows the time evolutions of the bending mode energy of HOD in the original ($s = 1$) and scaled ($s = 3$) trajectories calculated at the double precision. The bending energy does not relax but undergoes rapid oscillation through bend–stretch recurrence [152]. The time evolutions in the original and scaled trajectories are essentially the same up to ~5 ps, or equivalence is maintained. After this period, it looks as if dephasing occurs, which is actually caused by numerical chaos. The influence of the numerical chaos can be better seen by calculating many scaled trajectories and averaging the results at equivalent times. The averages over 1000 such trajectories calculated at the single (32-bit), double (64-bit), and extended double (128-bit) precisions are shown in Fig. 12. Even though the bending energy in each trajectory oscillates indefinitely (>1 ns), the trajectory averages dampen quickly as if IVR occurred. Improving the arithmetic precision extends the time interval which is effectively free from the influence of numerical chaos. But the improvement achieved is simply proportional to the number of digits used in the calculation while the computation time increases more rapidly. A simpler way to inspect the advent of numerical chaos is to calculate two initially equivalent trajectories (for example, $s = 1$ and 3) and evaluate E_q along the trajectories. The results are shown in Fig. 13. The trend here is the same as above. Namely, breakup of equivalence caused by numerical chaos occurs on a low picosecond time scale and improving the arithmetic precision is not an effective

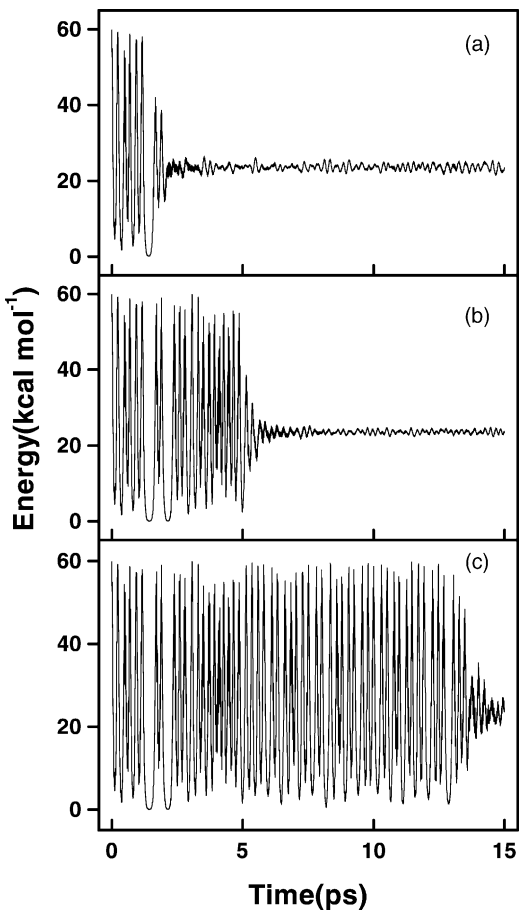

Fig. 12. Time evolution of the bending energy of HOD averaged over 1000 equivalent trajectories. The original trajectory ($s = 1$) was initiated at the phase angle of 229.15° and bending energy of 60 kcal mol^{-1}. Equivalent trajectories were calculated using 999 different scaling factors (s) other than 2^n. The mode energies in scaled calculations were rescaled. (a) Single, (b) double, and (c) extended double precision calculations. (Taken from ref. [125] with permission from Elsevier.)

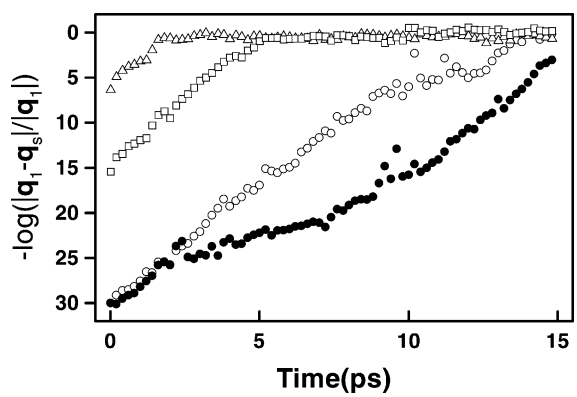

Fig. 13. Time evolution of $-\log(|\boldsymbol{q}_1 - \boldsymbol{q}_s|/|\boldsymbol{q}_1|)$ along trajectories of HOD at single (△), double (□), and extended double (○) precisions calculated with 0.01 fs time step. Solid circles (●) represent the extended double precision results calculated with 0.1 fs time step. Initial phase angle was 229.15° and initial bending energy was 60 kcal mol^{-1}. The scaled trajectory was run with $s = 3$. (Taken from ref. [125] with permission from Elsevier.)

way to slow it down. We attempted various other schemes to lengthen the useful time interval but failed.

Not added in proof

After the completion of the manuscript, it was found that some of the important contributions to the development of the classical trajectory methodology for the study of ion dissociation dynamics were not pointed out specifically. Additional references [153–163] are provided here so that the readers gain further overview of the field.

Acknowledgements

This work was supported by CRI, the Ministry of Science and Technology, Republic of Korea. A partially automated version of the software embodying most of the methods described in this review is available upon request. For the time being we are attempting a complete automation of the software.

References

[1] L.M. Raff, D.L. Thompson, in: M. Baer (Ed.), Theory of Chemical Reaction Dynamics, vol. 3, CRC Press, Boca Raton, FL 1985.
[2] T. Baer, Adv. Chem. Phys. 64 (1986) 111.
[3] M.T. Bowers (Ed.), Gas Phase Ion Chemistry, Academic Press, New York, 1979.
[4] R.D. Levine, R.B. Bernstein, Molecular Reactions Dynamics and Chemical Reactivity, Oxford University Press, New York, 1987.
[5] W. Forst, Theory of Unimolecular Reactions, Academic Press, New York, 1973.
[6] P.J. Robinson, K.A. Holbrook, Unimolecular Reactions, Wiley/Interscience, New York, 1972.
[7] R.A. Marcus, O.K. Rice, J. Phys. Colloid Chem. 55 (1951) 894.
[8] R.A. Marcus, J. Chem. Phys. 20 (1952) 364.
[9] R.A. Marcus, J. Chem. Phys. 20 (1952) 359.
[10] G.M. Wiedner, R.A. Marcus, J. Chem. Phys. 37 (1962) 1835.
[11] C.H. Kwon, M.S. Kim, J.C. Choe, J. Am. Soc. Mass Spectrom. 12 (2001) 1120.
[12] Y.Y. Youn, C.H. Kwon, J.C. Choe, M.S. Kim, J. Chem. Phys. 117 (2002) 2538.
[13] B.E. Miller, T. Baer, Chem. Phys. 85 (1984) 39.
[14] J.H.D. Eland, R. Frey, A. Kuestler, H. Schulte, B. Brehm, Int. J. Mass Spectrom. Ion Phys. 22 (1976) 155.
[15] J. Dannacher, A. Schmelzer, J.P. Stadelmann, J. Vogt, Int. J. Mass Spectrom. Ion Phys. 31 (1979) 175.
[16] G.K. Jarvis, K.J. Boyle, C.A. Mayhew, R.P. Tuckett, J. Phys. Chem. A 102 (1998) 3219.
[17] T. Nishimura, Q. Zha, G.G. Meisels, J. Chem. Phys. 87 (1987) 4589.
[18] K.M. Weitzel, F. Güethe, J. Mähnert, R. Locht, H. Baumgärtel, Chem. Phys. 201 (1995) 287.
[19] R.E. Krailler, D.H. Russell, Int. J. Mass Spectrom. Ion Process. 66 (1985) 339.
[20] T.L. Bunn, T. Baer, J. Chem. Phys. 85 (1986) 6361.
[21] D.Y. Kim, J.C. Choe, M.S. Kim, J. Chem. Phys. 113 (2000) 1714.
[22] D.S. Won, M.S. Kim, J.C. Choe, T.K. Ha, J. Chem. Phys. 115 (2001) 5454.
[23] K. Suto, Y. Sato, Y. Matsumi, M. Kawasaki, J. Phys. Chem. A 101 (1997) 1227.
[24] E. Teller, J. Phys. Chem. 41 (1937) 109.
[25] M. Desouter-Lecomte, D. Dehareng, B. Leyh-Nihant, M.T. Praet, A.J. Lorquet, J.C. Lorquet, J. Phys. Chem. 89 (1985) 214.
[26] A.L. Kaledin, Q. Cui, M.C. Heaven, K. Morokuma, J. Chem. Phys. 111 (1999) 5004.
[27] R.C. Gillen, B. Ostojic, W. Domcke, Chem. Phys. 272 (2001) 1.
[28] D.R. Yarkony, J. Phys. Chem. 100 (1996) 18612.
[29] M.S. Kim, C.H. Kwon, J.C. Choe, J. Chem. Phys. 113 (2000) 9532.
[30] W.G. Hwang, H.L. Kim, M.S. Kim, J. Chem. Phys. 113 (2000) 4153.
[31] S.T. Park, S.K. Kim, M.S. Kim, J. Chem. Phys. 115 (2001) 2492.
[32] S.T. Park, S.K. Kim, M.S. Kim, Nature 415 (2002) 306.
[33] S.T. Park, M.S. Kim, J. Am. Chem. Soc. 124 (2002) 7614.
[34] S.T. Park, M.S. Kim, J. Chem. Phys. 117 (2002) 124.
[35] R. Bombach, J. Dannacher, J.P. Stadelmann, J. Vogt, Chem. Phys. Lett. 77 (1981) 399.
[36] J. Dannacher, Org. Mass Spectrom. 19 (1984) 253.
[37] J.C. Choe, M.S. Kim, J. Phys. Chem. 95 (1991) 50.
[38] S.H. Lim, J.C. Choe, M.S. Kim, J. Phys. Chem. A 102 (1998) 7375.
[39] W.G. Hwang, J.H. Moon, J.C. Choe, M.S. Kim, J. Phys. Chem. A 102 (1998) 7512.
[40] S.T. Oh, J.C. Choe, M.S. Kim, J. Phys. Chem. 100 (1996) 13367.
[41] Y.H. Yim, M.S. Kim, J. Phys. Chem. 97 (1993) 12122.
[42] Y.H. Yim, M.S. Kim, J. Phys. Chem. 98 (1994) 5201.
[43] J. Laskin, C. Lifshitz, J. Mass Spectrom. 36 (2001) 459.
[44] R.G. Cooks, J.H. Beynon, R.M. Caprioli, G.R. Lester, Metastable Ions, Elsevier, Amsterdam, 1973.
[45] I.C. Yeh, M.S. Kim, Rapid. Commmun. Mass Spectrom. 6 (1992) 293.
[46] I.C. Yeh, M.S. Kim, Rapid. Commmun. Mass Spectrom. 6 (1992) 115.

[47] C. Lifshitz, Int. J. Mass Spectrom. Ion Phys. 118/119 (1992) 315.
[48] T. Baer, P.M. Mayer, J. Am. Soc. Mass Spectrom. 8 (1997) 103.
[49] H.M. Rosenstock, M.B. Wallenstein, A.L. Wahrhaftig, H. Eyring, Proc. Natl. Acad. Sci. U.S.A. 38 (1952) 667.
[50] H.M. Rosenstock, R. Stockbaucer, A.C. Parr, J. Chem. Phys. 71 (1979) 3708.
[51] C. Lifshitz, Adv. Mass Spectrom. 11 (1989) 713.
[52] W.J. Chesnavich, M.T. Bowers, J. Am. Chem. Soc. 98 (1976) 8301.
[53] W.J. Chesnavich, M.T. Bowers, J. Chem. Phys. 66 (1977) 2306.
[54] J.C. Choe, M.S. Kim, Int. J. Mass Spectrom. Ion Phys. 107 (1991) 103.
[55] P. Pechukas, J.C. Light, J. Chem. Phys. 42 (1965) 3281.
[56] C.E. Klots, J. Phys. Chem. 75 (1971) 1526.
[57] J.C. Light, J. Chem. Phys. 40 (1964) 3221.
[58] R.A. Marcus, J. Chem. Phys. 62 (1975) 1372.
[59] R.A. Marcus, Chem. Phys. Lett. 144 (1988) 208.
[60] R.E. Wyatt, J.Z. Zhang, Potential Energy Surfaces and Dynamics Calculations, Plenum Press, New York, 1981.
[61] R. Kosloff, J. Phys. Chem. 92 (1988) 2087.
[62] D.C. Clary, J. Echave, Advances in Molecular Vibrations and Collision Dynamics, JAI Press, Stanford, CN, 1994.
[63] J.M. Bowman, G.C. Schatz, Annu. Rev. Phys. Chem. 46 (1995) 169.
[64] Q. Sun, J.M. Bowman, Int. J. Quant. Chem. s23 (1989) 115.
[65] W.H. Miller, Acc. Chem. Res. 26 (1993) 174.
[66] W.H. Miller, Annu. Rev. Phys. Chem. 41 (1990) 245.
[67] D.C. Clary, J. Phys. Chem. 98 (1994) 10678.
[68] F. Huarte-Larranaga, U. Manthe, J. Chem. Phys. 113 (2000) 5115.
[69] H. Szichman, R. Baer, J. Chem. Phys. 117 (2002) 7614.
[70] T.D. Sewell, D.L. Thompson, Int. J. Modern Phys. B 11 (1997) 1067.
[71] T.G. Lee, S.C. Park, M.S. Kim, J. Chem. Phys. 104 (1996) 4517.
[72] P.R. Bunker, M. Kofranek, H. Lischka, A. Karpfen, J. Chem. Phys. 89 (1988) 3002.
[73] S.A. Abrash, R.W. Zehner, G.J. Mains, L.M. Raff, J. Phys. Chem. 99 (1995) 2959.
[74] G.C. Lynch, D.G. Truhlar, F.B. Brown, J.G. Zhao, J. Phys. Chem. 99 (1995) 207.
[75] Y. Amatatsu, S. Yabushita, K. Morokuma, J. Chem. Phys. 104 (1996) 9783.
[76] M.A. ter Horst, G.C. Schatz, L.B. Harding, J. Chem. Phys. 105 (1996) 558.
[77] M.J. Frisch, G.W. Trucks, H.B. Schlegel, G.E. Scuseria, M.A. Robb, J.R. Cheeseman, V.G. Zakrzewski, J.A. Montgomery, Jr., R.E. Stratmann, J.C. Burant, S. Dapprich, J.M. Millam, A.D. Daniels, K.N. Kudin, M.C. Strain, O. Farkas, J. Tomasi, V. Barone, M. Cossi, R. Cammi, B. Mennucci, C. Pomelli, C. Adamo, S. Clifford, J. Ochterski, G.A. Petersson, P.Y. Ayala, Q. Cui, K. Morokuma, D.K. Malick, A.D. Rabuck, K. Raghavachari, J.B. Foresman, J. Cioslowski, J.V. Ortiz, B.B. Stefanov, G. Liu, A. Liashenko, P. Piskorz, I. Komaromi, R. Gomperts, R.L. Martin, D.J. Fox, T. Keith, M.A. Al-Laham, C.Y. Peng, A. Nanayakkara, C. Gonzalez, M. Challacombe, P.M.W. Gill, B. Johnson, W. Chen, M.W. Wong, J.L. Andres, C. Gonzalez, M. Head-Gordon, E.S. Replogle, J.A. Pople, Gaussian 98, Revision A.6, Gaussian, Inc., Pittsburgh, PA, 1998.
[78] M.W. Schmidt, K.K. Baldridge, J.A. Boatz, S.T. Elbert, M.S. Gordon, J.J. Jensen, S. Koseki, N. Matsunaga, K.A. Nguyen, S. Su, T.L. Windus, M. Dupuis, J.A. Montgomery, J. Comput. Chem. 14 (1993) 1347.
[79] T. Helgaker, E. Uggerud, H.J.A. Jensen, Chem. Phys. Lett. 173 (1990) 145.
[80] W. Chen, W.L. Hase, H.B. Schlegel, Chem. Phys. Lett. 228 (1994) 436.
[81] E. Uggerud, Mass Spectrom. Rev. 18 (1999) 285.
[82] R. Car, M. Parrinello, Phys. Rev. Lett. 55 (1985) 2471.
[83] M. Tuckerman, K. Laasonen, M. Sprik, M. Parrinello, J. Phys. Chem. 99 (1995) 5749.
[84] M.E. Tuckerman, P.J. Ungar, T. von Rosenvinge, M.L. Klein, J. Phys. Chem. 100 (1996) 12878.
[85] M.E. Tuckerman, G.J. Martyna, J. Phys. Chem. B 104 (2000) 159.
[86] D.G. Truhlar, R. Steckler, M.S. Gordon, Chem. Rev. 87 (1987) 217.
[87] G.C. Schatz, Rev. Modern Phys. 61 (1989) 669.
[88] J. Ischtwan, M.A. Collins, J. Chem. Phys. 100 (1994) 8080.
[89] T. Hollebeek, T.S. Ho, H. Rabitz, Annu. Rev. Phys. Chem. 50 (1999) 537.
[90] T.S. Ho, T. Hollebeek, H. Rabitz, S.D. Chao, R.T. Skodje, A.S. Zyubin, A.M. Mebel, J. Chem. Phys. 116 (2002) 4124.
[91] J.M. Geremia, H. Rabitz, J. Chem. Phys. 115 (2001) 8899.
[92] T. Hollebeek, T.S. Ho, H. Rabitz, L.B. Harding, J. Chem. Phys. 114 (2001) 3945.
[93] L.A. Pederson, G.C. Schatz, T. Hollebeek, H. Rabitz, L.B. Harding, J. Phys. Chem. A 104 (2000) 2301.
[94] L.A. Pederson, G.C. Schatz, T.S. Ho, T. Hollebeek, H. Rabitz, L.B. Harding, G.R. Lendvay, J. Chem. Phys. 110 (1999) 9091.
[95] M.J.T. Jordan, K.C. Thompson, M.A. Collins, J. Chem. Phys. 102 (1995) 5647.
[96] M.J.T. Jordan, K.C. Thompson, M.A. Collins, J. Chem. Phys. 103 (1995) 9669.
[97] M.J.T. Jordan, M.A. Collins, J. Chem. Phys. 104 (1996) 4600.
[98] K.C. Thompson, M.A. Collins, J. Chem. Soc., Faraday Trans. 93 (1997) 871.
[99] K.C. Thompson, M.J.T. Jordan, M.A. Collins, J. Chem. Phys. 108 (1998) 8302.
[100] R.P.A. Betten, M.A. Collins, J. Chem. Phys. 108 (1998) 2424.
[101] K.A. Nguyen, I. Rossi, D.G. Truhlar, J. Chem. Phys. 103 (1995) 5522.
[102] Y.M. Rhee, T.G. Lee, S.C. Park, M.S. Kim, J. Chem. Phys. 106 (1997) 1003.
[103] T. Ishida, G.C. Schatz, J. Chem. Phys. 107 (1997) 3558.
[104] C. Gonzalez, H.B. Schlegel, J. Chem. Phys. 90 (1989) 2154.

[105] C. Gonzalez, H.B. Schlegel, J. Phys. Chem. 94 (1990) 5523.
[106] K.C. Thompson, T.J. Martinez, J. Chem. Phys. 110 (1999) 1376.
[107] S.Y. Lin, S.C. Park, M.S. Kim, J. Chem. Phys. 111 (1999) 3787.
[108] K.C. Thompson, M.J.T. Jordan, M.A. Collins, J. Chem. Phys. 108 (1998) 564.
[109] Y.M. Rhee, J. Chem. Phys. 113 (2000) 6021.
[110] R. Farwig, Algorithms for Approximation, Clarendon Press, Oxford, 1987.
[111] P. Lancaster, K. Salkauskas, Curve and Surface Fitting, An Introduction, Academic Press, Oxford, 1986.
[112] D. Yarkony, J. Am. Chem. Soc. 114 (1992) 5406.
[113] E. Uggerud, T. Helgaker, J. Am. Chem. Soc. 114 (1992) 4265.
[114] G. Hvistendahl, E. Uggerud, Org. Mass Spectrom. 20 (1985) 541.
[115] G. Hvistendahl, E. Uggerud, Org. Mass Spectrum. 26 (1991) 67.
[116] D. Suárez, T.L. Sordo, J. Phys. Chem. A 101 (1997) 1561.
[117] T.G. Lee, M.S. Kim, S.C. Park, J. Chem. Phys. 104 (1996) 5472.
[118] Y.M. Rhee, M.S. Kim, J. Chem. Phys. 109 (1998) 5363.
[119] J.H. Moon, S.T. Park, M.S. Kim, J. Chem. Phys. 110 (1999) 972.
[120] D.L. Bunker, W.L. Hase, J. Chem. Phys. 59 (1973) 4621.
[121] W.L. Hase, D.G. Buckowski, Chem. Phys. lett. 74 (1980) 284.
[122] W.H. Press, S.A. Teukolsky, W.T. Vettering, B.P. Flannery, Numerical Recipes in FORTRAN, 2nd ed., Cambridge University Press, Cambridge, 1992.
[123] L.F. Shampine, Numerical Solution of Ordinary Differential Equations, Chapman & Hall, New York, 1994.
[124] G. Hall, J.M. Watt, Modern Numerical Methods for Ordinary Differential Equations, Clarendon Press, Oxford, 1976.
[125] B.J. Sung, J.H. Moon, M.S. Kim, Chem. Phys. Lett. 342 (2001) 610.
[126] S.T. Park, J.H. Moon, M.S. Kim, J. Chem. Phys. 107 (1997) 9899.
[127] J.E.B. Wilson, J.C. Decius, P.C. Cross, Molecular Vibrations, McGraw-Hill, New York, 1955.
[128] S. Califano, Vibrational States, Wiley, New York, 1976.
[129] Y.M. Rhee, M.S. Kim, J. Chem. Phys. 107 (1997) 1394.
[130] B.J. Sung, M.S. Kim, J. Chem. Phys. 113 (2000) 3098.
[131] T.H. Choi, S.T. Park, M.S. Kim, J. Chem. Phys. 114 (2001) 6051.
[132] M.S. Kim, S.T. Park, B.J. Sung, J.H. Moon, J. Chem. Phys. 114 (2001) 10583.
[133] P. Ho, D.J. Bamford, R.J. Buss, Y.T. Lee, C.B. Moore, J. Chem. Phys. 76 (1982) 3630.
[134] D.J. Bamford, S.V. Filseth, M.F. Foltz, J.W. Hepburn, C.B. Moore, J. Chem. Phys. 82 (1985) 3032.
[135] D. Debarre, M. Lefebvre, M.Péalat, J.P.E. Taran, D.J. Bamford, C.B. Moore, J. Chem. Phys. 83 (1985) 4476.
[136] T.J. Butenhoff, K.L. Carleton, C.B. Moore, J. Chem. Phys. 92 (1990) 377.
[137] W.H. Miller, J. Am. Chem. Soc. 101 (1979) 6810.
[138] J. Troe, J. Phys. Chem. 88 (1984) 4375.
[139] R.V. Jensen, Am. Scientist 75 (1987) 168.
[140] A.S. deMarkus, Phys. Rev. E 56 (1997) 88.
[141] A.S. deMarkus, Phys. Rev. E 55 (1997) 1342.
[142] A.S. deMarkus, R.E. Mickens, J. Comp. Appl. Math. 106 (1999) 317.
[143] K. Shida, R. Suzuki, T. Kawai, Comp. Phys. Commun. 102 (1997) 59.
[144] D.J. Kouri, D.S. Zhang, G.W. Wei, T. Konshak, D.K. Hoffman, Phys. Rev. E 59 (1999) 1274.
[145] M.J. Ablowitz, C. Schober, B.M. Herbst, Phys. Rev. Lett. 71 (1993) 2683.
[146] D.J. Nesbitt, R.W. Field, J. Phys. Chem. 100 (1996) 12735.
[147] K.N. Swamy, W.L. Hase, J. Chem. Phys. 82 (1985) 123.
[148] K. Bolton, S. Nordholm, Chem. Phys. 203 (1996) 101.
[149] R.E. Wyatt, J. Chem. Phys. 109 (1998) 10732.
[150] T.J. Minehardt, R.E. Wyatt, J. Chem. Phys. 109 (1998) 8330.
[151] D. Bingemann, M.P. Gorman, A.M. King, F.F. Crim, J. Chem. Phys. 107 (1997) 661.
[152] M.S. Kim, S.T. Park, S.Y. Kwon, H.L. Kim, Chem. Phys. Lett. 322 (2000) 351.
[153] M. Igarashi, H. Tachikawa, Int. J. Mass Spectrom. 181 (1998) 151.
[154] H. Tachikawa, M. Igarashi, Chem. Phys. Lett. 303 (1999) 81.
[155] H. Tachikawa, J. Phys. Chem. A 104 (2000) 497.
[156] H. Tachikawa, J. Phys. Chem. A 105 (2001) 1260.
[157] D.J. Mann, W.L. Hase, J. Phys. Chem. A 102 (1998) 6208.
[158] L. Sun, W.L. Hase, K. Song, J. Am. Chem. Soc. 123 (2001) 5753.
[159] H. Wang, W.L. Hase, Int. Mass Spectrom. Ion Process 167/168 (1997) 573.
[160] T. Su, H. Wang, W.L. Hase, J. Phys. Chem. A 102 (1998) 9819.
[161] S.O. Meroueh, Y. Wang, W.L. Hase, J. Phys. Chem. A 106 (2002) 9983.
[162] W.L. Hase, R.J. Duchovic, X. Hu, A. Komornicki, K.F. Lim, D.-H. Lu, G.H. Peslherbe, K.N. Swamy, S.R. Vande Linde, A. Varandas, H. Wang, R.J. Wolf, QCPE 16 (1996) 671.
[163] G.H. Peslherbe, H.B. Wang, W.L. Hase, Adv. Chem. Phys. 105 (1999) 171.